



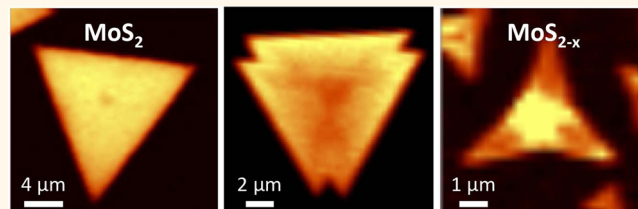
ARRCI
J

Influence of Stoichiometry on the Optical and Electrical Properties of Chemical Vapor Deposition Derived MoS₂

In Soo Kim,[†] Vinod K. Sangwan,[†] Deep Jariwala,[†] Joshua D. Wood,[†] Spencer Park,[†] Kan-Sheng Chen,[†] Fengyuan Shi,[†] Francisco Ruiz-Zepeda,^{||} Arturo Ponce,^{||} Miguel Jose-Yacaman,^{||} Vinayak P. Dravid,^{†,‡} Tobin J. Marks,^{†,‡} Mark C. Hersam,^{*,†,‡,§} and Lincoln J. Lauhon^{*,†}

[†]Department of Materials Science and Engineering, Northwestern University, Evanston, Illinois 60208, United States, [‡]Department of Chemistry, Northwestern University, Evanston, Illinois 60208, United States, [§]Department of Medicine, Northwestern University, Evanston, Illinois 60208, United States, ^{||}International Institute of Nanotechnology, Northwestern University, Evanston, Illinois 60208, United States, and ^{||}Department of Physics and Astronomy, University of Texas at San Antonio, San Antonio, Texas 78249, United States

ABSTRACT Ultrathin transition metal dichalcogenides (TMDCs) of Mo and W show great potential for digital electronics and optoelectronic applications. Whereas early studies were limited to mechanically exfoliated flakes, the large-area synthesis of 2D TMDCs has now been realized by chemical vapor deposition (CVD) based on a sulfurization reaction. The optoelectronic properties of CVD grown monolayer MoS₂ have been intensively investigated, but the



influence of stoichiometry on the electrical and optical properties has been largely overlooked. Here we systematically vary the stoichiometry of monolayer MoS₂ during CVD via controlled sulfurization and investigate the associated changes in photoluminescence and electrical properties. X-ray photoelectron spectroscopy is employed to measure relative variations in stoichiometry and the persistence of MoO_x species. As MoS_{2-δ} is reduced (increasing δ), the field-effect mobility of monolayer transistors increases while the photoluminescence yield becomes nonuniform. Devices fabricated from monolayers with the lowest sulfur content have negligible hysteresis and a threshold voltage of ~0 V. We conclude that the electrical and optical properties of monolayer MoS₂ crystals can be tuned via stoichiometry engineering to meet the requirements of various applications.

KEYWORDS: transition metal dichalcogenides · molybdenum disulfide · chemical vapor deposition · stoichiometry · photoluminescence · field-effect mobility · X-ray photoelectron spectroscopy

The physical properties of electronic materials can be usefully controlled by tuning stoichiometry and doping. In conventional semiconductors like silicon, doping improves the electrical conductivity by increasing carrier concentration without significantly degrading carrier mobility.¹ However, doping of reduced dimensionality semiconductors without degrading mobility has proven challenging due to confined channel dimensions and increased scattering cross-section of carriers, as seen in reduced dimensionality carbon allotropes such as carbon nanotubes and graphene.² Similar challenges arise for the layered transition metal dichalcogenides (TMDCs) of Mo and W. Mono- and few-layer TMDCs exhibit bandgaps that can be tuned by thickness,

strain, and composition, making them promising 2D semiconductors complementary to graphene and hexagonal boron nitride in various optoelectronic applications.³ The electrical and optical properties of TMDCs are particularly sensitive to surrounding interfaces,^{4–8} as well as intrinsic and extrinsic defects such as chalcogen vacancies^{9,10} and dopants,^{11–13} respectively. Consequently, defect engineering through controlled synthesis and post-synthesis processing provides a facile means to tune physical properties.

Several CVD-based methods have been developed to synthesize MoS₂ over large areas, including sulfurization of e-beam evaporated thin Mo metal films,¹⁴ decomposition of ammonium thiomolybdate ((NH₄)₂MoS₄),¹⁴ direct vapor phase deposition of MoS₂

* Address correspondence to lauhon@northwestern.edu, m-hersam@northwestern.edu.

Received for review July 19, 2014 and accepted September 15, 2014.

Published online September 15, 2014
10.1021/nn503988x

© 2014 American Chemical Society

powder,¹⁵ and sulfurization of molybdenum trioxide (MoO_3) using elemental sulfur.^{16–18} Among these methods, the sulfurization of MoO_3 has been the most widely adopted. Because varying degrees of sulfurization during growth may lead to varying concentrations of both intentional and unintentional point defects, such as vacancies and dopants, it is important to establish the influence of materials processing conditions on physical properties. For example, the field-effect mobility of both mechanically exfoliated and as-synthesized CVD MoS_2 monolayer crystals, hereafter referred to as “flakes”, is an order of magnitude lower than the intrinsic limits.^{19,20} Variations in carrier mobilities and charge transport mechanisms in CVD MoS_2 have been variously attributed to trapped charges at sulfur vacancies,¹⁴ trapped charges at the interface of MoS_2 and oxide dielectrics,²¹ extrinsic disorder from adsorbates,^{20,22} grain boundaries,¹⁷ and other defects within the films.^{3,18,20,23} However, charge transport in CVD MoS_2 has not been investigated in concert with systematic variations in stoichiometry.

In this work, we correlate stoichiometry with the electrical properties of CVD synthesized monolayer MoS_2 flakes prepared under varying degrees of MoO_3 sulfurization. X-ray photoelectron spectroscopy shows that an increase in the degree of sulfurization leads to an improvement in the relative stoichiometry and a decrease in the amount of $\text{MoO}_3/\text{MoO}_x$ within the region probed. Approaching stoichiometric MoS_2 , the photoluminescence becomes spatially more uniform while the electrical transport becomes more resistive with large hysteresis in gate bias sweeps. Surprisingly, the least stoichiometric samples show up to an order of magnitude higher field-effect mobilities, negligible hysteresis, and threshold voltages close to 0.0 V. An inverse correlation between stoichiometry and standard transistor metrics is established among a set of three different growth conditions, demonstrating the potential to optimize stoichiometry for various device applications.

RESULTS AND DISCUSSION

To investigate the effects of stoichiometry on the optical and electrical properties of monolayer MoS_2 flakes, three groups of samples were prepared (Table 1) by modifying previously described growth procedures.^{16–18} Briefly, MoO_3 and S powder sources were evaporated at 800 and 150 °C, respectively. The sulfur source was loaded sequentially in a total of four steps to prevent premature sulfurization of the MoO_3 source and to ensure sufficient sulfurization throughout the growth (see details in Methods). The degree of sulfurization was controlled by varying the time of exposure to sulfur vapor and the temperature of sulfur source as tabulated in Table 1.

Individual monolayer MoS_2 flakes of all the samples grown on SiO_2/Si (300 nm) are readily identified by the

TABLE 1. Variation in Growth Conditions for Intentional Modification of Stoichiometry in MoS_2 Flakes

	group A	group B	group C
exposure to sulfur vapor (min)	10	10	3
temperature of sulfur (°C)	170	150	150

optical contrast arising from thin film interference (Figure 1a). Atomic force microscopy (AFM) was used to determine the absolute thickness of individual flakes as well as to visualize thickness variations and grain boundaries within flakes. A thickness of ~5 Å was extracted from the height profile of the AFM topography image of an individual MoS_2 flake (Figure 1b), in line with previous reports.^{4,24–26} Interestingly, the grain boundaries in mono- and bilayer regions exhibit a sharp contrast in the AFM phase image (Figure 1c and Supporting Information). Brightness and contrast of the bilayer region was adjusted to distinguish mono- and bilayer regions. Similar grain boundaries in MoS_2 flakes have been visualized with transmission electron microscopy (TEM); however, the AFM imaging shown here enables rapid and nondestructive imaging of atomically thin grain boundaries. The local atomic structure of a flake consisting of both mono- and bilayer MoS_2 was next examined by aberration (C_s) corrected scanning transmission electron microscopy (STEM) in a JEOL ARM 200F instrument operated at 80 kV. The crystal is flat and a 6-fold symmetry was confirmed directly from the STEM image with lattice spacing of 3.1 ± 1 Å (Figure 1d). In the high angular dark field (HAADF) image, the contrast is proportional to the square of the atomic number, and atomic positions of molybdenum and sulfur atoms can be distinguished; Mo atoms show higher contrast than S atoms. This enables identification of the stacking sequence in MoS_2 bilayers. The Raman spectrum in Figure 1e of monolayer MoS_2 exhibits characteristic E_{2g}^1 and A_{1g} modes associated with in-plane and out-of plane vibrations. The two peaks appear at ~383.8 and 404.4 cm^{-1} , resulting in the frequency difference of ~ 20.6 cm^{-1} , consistent with the values reported in literature for CVD monolayer MoS_2 flakes. A strong luminescence band located at 678 nm (excitation wavelength at 532 nm) shown in Figure 1f corresponds to the A direct excitonic transition,²⁷ indicative of a monolayer MoS_2 flake with a direct 1.83 eV band gap.

Photoluminescence and Raman Microspectroscopy. Representative variations in the photoluminescence and Raman spectra within flakes and between sample groups are shown in Figure 2. Photoluminescence emission and Raman E_{2g}^1 mode scattering maps were constructed by integrating the respective emission and scattering intensities. Multiple samples were investigated from each of the groups to establish a representative data set. Group A samples (highest sulfur exposure) exhibit spatially uniform emission

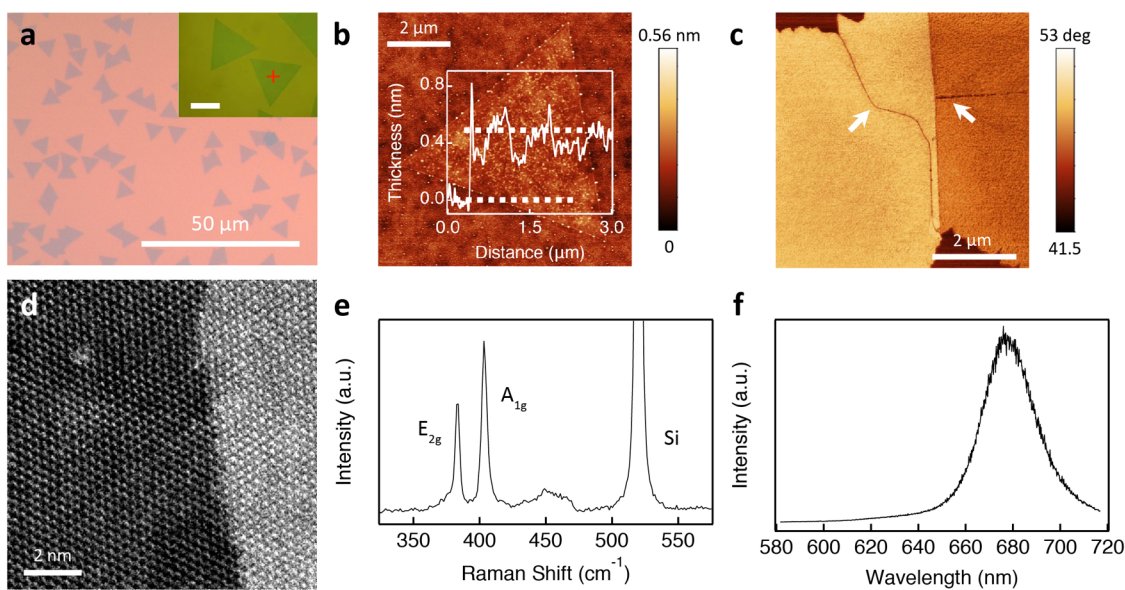


Figure 1. (a) Optical image of monolayer MoS₂ flakes. Inset is a higher magnification image. The cross hair indicates where Raman and photoluminescence spectra were acquired. Scale bar 10 μm . (b) AFM topography image of isolated monolayer MoS₂ and corresponding height profile (inset). (c) AFM phase image of a MoS₂ flake consisting of mono- and bilayer regions with grain boundaries marked by white arrows. Bilayer region is distinguished by the dark contrast. (d) High-angle annular dark field (HAADF) STEM image resolving the atomic structure. The image was recorded using a convergence angle of 25 mrad with a probe size of about 0.09 nm. (e and f) Representative Raman and photoluminescence spectra of monolayer MoS₂.

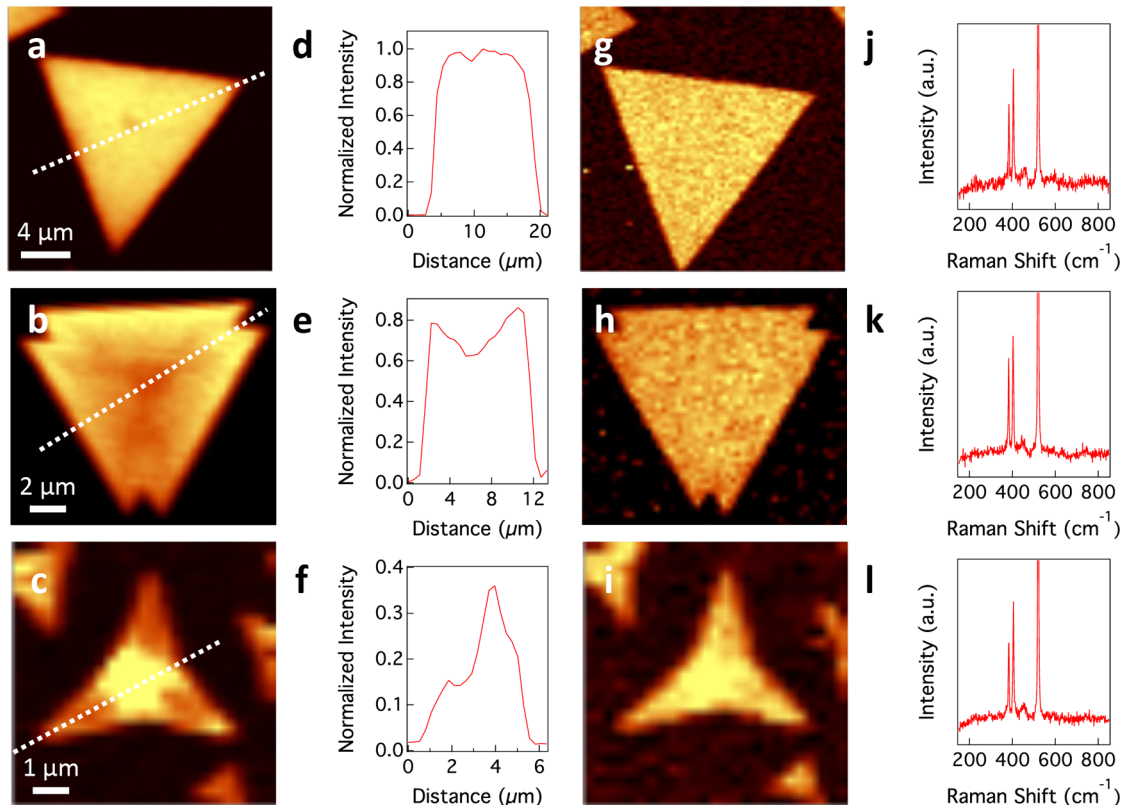


Figure 2. (a–c) Integrated photoluminescence intensity maps for samples from group A, B, and C, respectively. (d–f) Normalized intensity line profiles extracted from photoluminescence maps. (g–i) Corresponding Raman maps constructed by integrating E_{12g} mode. (j–l) Representative Raman spectra for the three different growth conditions.

intensity and strong emission peaked at \sim 678 nm (Figure 2a,d). The peak emission wavelength and full width at half-maximum (fwhm) vary less than 0.4 nm

across the flake. In contrast, the group C sample (least sulfur exposure) exhibits in-plane variations in emission intensity (Figure 2c,f), with the emission intensity

in the central region ~ 3 times higher than that of the edge regions, but only $\sim 35\%$ of that of the group A sample. Furthermore, the center emission is slightly red-shifted, although no strong correlation is observed between the emission intensity and wavelength. The full width at half-maximum (fwhm) of the emission peaks is comparable between sample groups. The photoluminescence intensity of the group B samples is comparable to that of the group A samples, but the intensity decreases moving toward the center of the flake (Figure 2b,d).

Many factors may influence photoluminescence characteristics including defects (vacancies, grain boundaries), strain, and electrostatic doping.^{17,28} Raman spectroscopy was used to rule out strain and electrostatic doping as primary causes of the variations in emission intensity; the frequency of E_{2g}^1 vibrational mode is sensitive to strain,²⁹ whereas the frequency of A_{1g} vibrational mode is sensitive to electrostatic doping.³⁰ Raman maps of the E_{2g}^1 peak center of mass are quite uniform (Figure 2g–i), and are comparable to similar maps of the A_{1g} mode. Integrated peak intensities and fwhm are also uniform, indicating that strain and electrostatic doping are negligible. We do not observe Raman signatures from oxide phases (MoO_3 and/or MoO_x) that would indicate the presence of residual oxygen associated with incomplete sulfurization (Figure 2 j,k,l). The possible contribution of sulfur vacancies to the nonuniform photoluminescence characteristics is discussed below.

Analysis of Stoichiometry by X-ray Photoelectron Spectroscopy (XPS). XPS analyses of the three groups of samples establish systematic variations in stoichiometry associated with the distinct processing conditions (Figure 3). To compensate for sample charging, all spectra were charge corrected against the C 1s adventitious carbon peak at 284.8 eV. In Mo 3d spectra of the group A (most stoichiometric) sample, both Mo^{4+} and Mo^{6+} doublets are observed. Mo^{4+} $3d_{5/2}$ and $3d_{3/2}$ doublet peaks appear at ~ 229.8 and ~ 233.0 eV with fwhm of ~ 1.23 eV (Figure 3a). The doublet peaks of Mo^{4+} $3d_{5/2}$ and $3d_{3/2}$ were deconvoluted into two components to obtain a good fit. The first set of components, located at 229.5 and 232.7 eV, corresponds to stoichiometric intrinsic MoS_2 (i- MoS_2). The second set of components located at slightly lower binding energies of 229.2 and 232.2 eV correspond to defective/substoichiometric MoS_2 (d- MoS_2) with sulfur vacancies. The third component located under Mo^{4+} $3d_{3/2}$ doublet and the broad peak (232.6 and ~ 236.0 eV) represents Mo^{6+} $3d_{5/2}$ and $3d_{3/2}$ doublets of MoO_3 ^{31,32} or MoO_x suboxides,³³ respectively. While we did not find evidence of $\text{MoO}_3/\text{MoO}_x$ within individual flakes from Raman mapping, the presence of $\text{MoO}_3/\text{MoO}_x$ in XPS likely arises from the large probe size ($\sim 400 \mu\text{m}$ diameter), which results in sampling of extended regions enclosing thicker regions of MoS_2 that may have incompletely sulfurized.

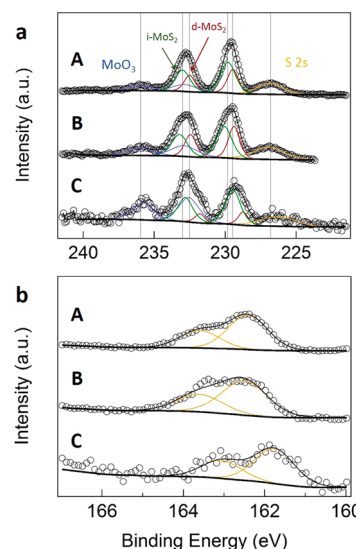


Figure 3. X-ray photoelectron spectra (XPS) for different CVD MoS_2 growth conditions. (a) Mo 3d and (b) S 2p core level spectra for CVD MoS_2 flakes on SiO_2/Si . Chemical contributions from MoO_3 , intrinsic MoS_2 (i- MoS_2), and defective MoS_2 (d- MoS_2) are shown.

We further note that the degree of inhomogeneity across the area sampled by XPS likely exceeds the degree of inhomogeneity within a single flake.

As expected, the presumed substoichiometric samples exhibit noticeable changes in their XPS spectra. First, shifts to lower binding energies were observed for the Mo^{4+} $3d_{5/2}$ and $3d_{3/2}$ doublet peaks, which reflect reduction of MoS_2 consistent with the presence of sulfur vacancies.^{34,35} A similar behavior was observed previously through preferential sputtering of sulfur from MoS_2 .^{34,35} When the doublets of the group B sample are decomposed using the same components used for the group A sample, the contribution of the intrinsic MoS_2 (i- MoS_2) decreases, whereas the defective MoS_2 (d- MoS_2) component increases. Second, the $\text{MoO}_3/\text{MoO}_x$ component is larger in the group C sample, indicating the presence of nonstoichiometric MoS_2 from incomplete sulfurization of $\text{MoO}_3/\text{MoO}_x$, and the increase in fwhm to ~ 1.27 eV indicates a higher degree of disorder in the substoichiometric group C sample. Finally, the decreased integrated area of the S 2s peak with respect to the Mo 3d peaks indicates a reduction in the total amount of sulfur as compared with the group A sample.

Transport Measurements. To investigate the effects of stoichiometry on the transport properties of CVD MoS_2 , two- and four-terminal devices were fabricated on individual, isolated MoS_2 flakes without grain boundaries using 2 nm Ti/70 nm Au metal contacts. An optical image of a representative four-terminal MoS_2 device (group A) in Figure 4a shows the trapezoidal channel for van der Pauw measurements. All devices were measured at room temperature at pressures of $\sim 2 \times 10^{-5}$ Torr. The majority of devices were fabricated and measured in a two-terminal geometry, while four-terminal measurements of a selected subset of

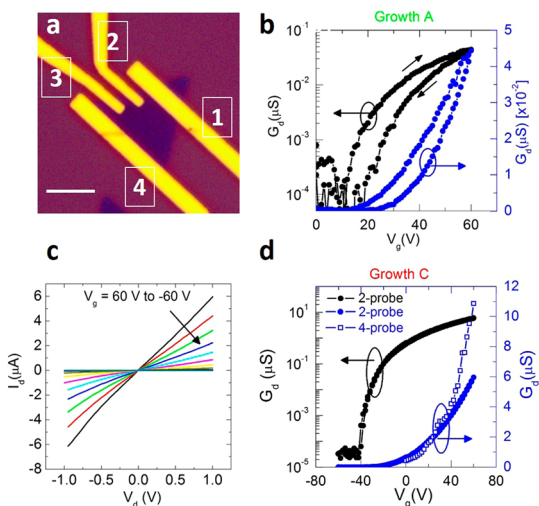


Figure 4. (a) Optical image of a 4-probe MoS₂ device (growth A). Scale bar is 4 μm . (b) Two-terminal transfer characteristics of the device measured between electrode "1" and "4" at V_d = 50 mV in linear as well as semilog plots. (c) Output I_d – V_d characteristics of a growth C device at V_g = 60 to –60 V. (d) Conductance (G_d) versus gate voltage (V_g) of the same device. Both two-terminal and four-terminal conductance are shown.

devices were conducted to assess the influence of contact resistance on mobility estimates and transistor characteristics (Supporting Information Table 1). Due to the large impedance in the subthreshold regime (see Methods), four-terminal van der Pauw measurements were conducted in the low impedance accumulation regime ($V_g > V_{th}$).

In general, as-fabricated group A devices had the lowest field-effect mobilities and largest hysteresis among samples considered here (Supporting Information Table 1). Figure 4b shows transfer characteristics (channel conductance *versus* gate voltage) of one device (114-S1, see Supporting Information Table 1) after conducting a current-annealing procedure, which was found to improve the device characteristics as discussed further below and in Supporting Information Section 2. The field-effect mobility (μ_{FE}) was calculated from the transfer curves based on the relation:

$$\mu_{FE} = \frac{dI_d}{dV_g} \left[\frac{L}{WC_i V_d} \right]$$

where I_d , V_g , and V_d are the drain current, gate voltage, and drain voltage, respectively; L is the length and W is the width of the channel; and $\sim 11 \text{ nF/cm}^2$ is assumed for the area normalized capacitance, C_i , of the 300 nm thick SiO₂. The field-effect mobility of six *as-fabricated* group A devices are in the range of 5×10^{-3} to $1.5 \text{ cm}^2/(\text{V s})$, while the average value ($0.48 \text{ cm}^2/(\text{V s})$) is comparable to values reported in literature.^{16,17}

Compared to exfoliated MoS₂, Group A devices show larger hysteresis,⁵ larger threshold voltages (average V_{th} = 40.8 V), and lower I_{ON}/I_{OFF} ratios ($\sim 10^4$).⁵ Furthermore, nonlinear output characteristics at low

biases in as-fabricated devices suggested the presence of a Schottky barrier at the contacts (Supporting Information Section 2). As a result, highly resistive as-fabricated devices could not be probed *via* four-terminal van der Pauw measurements. However, the transport characteristics of group A devices could be improved *via* current-annealing in vacuum as discussed in Supporting Information Section 2. Following annealing, the average field-effect mobility of the more resistive devices was increased by up to 2 orders of magnitude (e.g., from 5×10^{-3} to $0.16 \text{ cm}^2/(\text{V s})$ for sample 114-S1 in Supporting Information Table 1). Although current annealing also improves the linearity of I – V curves, they remain less linear than those of exfoliated MoS₂ flakes⁵ and the sulfur-deficient CVD MoS₂ samples discussed below (Supporting Information Figures S1c and S2a). The relative enhancement in device performance by current-annealing, which presumably involves Joule heating, is consistent with a recent report on thermal annealing of MoS₂.³⁶

Group B samples with a lower sulfur content (Figure 3) show slightly higher field-effect mobilities (0.2 – $3.8 \text{ cm}^2/(\text{V s})$), lower threshold voltages, and reduced hysteresis (Supporting Information Figure S3 and Table 1) compared to group A samples. The average field-effect mobility, threshold voltage, and I_{ON}/I_{OFF} ratio values of six group B devices are $2.66 \text{ cm}^2/(\text{V s})$, 34.8 V, and $\sim 10^5$, respectively. Group C samples, which are the least stoichiometric, showed a continued trend in electrical characteristics. A representative two-terminal device exhibits linear output characteristics at low biases (Figure 4c), suggesting that the contacts are improved compared to group A and B devices.^{4,37} Significantly improved transport characteristics of the group C devices are also evident in the linear and semilog transfer curves of the same device for both two- and four-terminal measurements (Figure 4d). First, compared with groups A and B, the field-effect mobilities of group C devices are larger by approximately by an order of magnitude, in the range of 12 – $21 \text{ cm}^2/(\text{V s})$ with an average mobility of $15.3 \text{ cm}^2/(\text{V s})$. This is the highest value reported for *as-synthesized* unencapsulated CVD monolayer MoS₂ flakes without current or thermal annealing. Furthermore, the threshold voltage shifted toward negative bias to an average of 12.3 V, which is indicative of increased *n*-type doping. The I_{ON}/I_{OFF} ratio was also improved to $\sim 10^6$ without noticeable hysteresis, consistent with the generally better transistor performance of the group C samples.

A comparison of the transfer characteristics of devices from the three growth conditions associates an increase in the average field-effect mobility and decrease in the threshold voltage with decreasing S content (Figure 5). As a proxy for direct composition measurements, we plot the ratio of the integrated S and MoO₃/MoO_x peaks for the three growth conditions

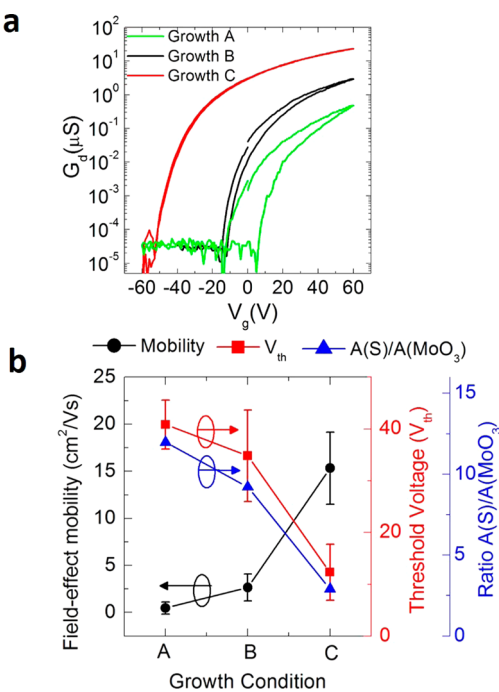


Figure 5. (a) G_d versus V_g ($V_d = 0.5$ V) of typical devices from growth A, B, and C. (b) Comparison of field-effect mobility, threshold voltage (V_{th}), and the normalized ratio of the S 2p and MoO_3 3d XPS core level areas with growth condition.

In Figure 5b, normalized against the relative sensitivity factors for the respective core levels. Considering Figures 4 and 5 together, we conclude that n-type conductivity, field-effect mobility, doping, and $I_{\text{ON}}/I_{\text{OFF}}$ ratio increase with decreasing stoichiometry. The increase in electron doping can be explained by an increasing concentration of sulfur vacancies acting as electron donors, but it is perhaps surprising that the field-effect mobility also increases.^{9,10} Below we examine whether the PL data are also consistent with the proposed variation in sulfur vacancy concentration, and then consider possible explanations for the trends in field effect mobility.

In general, structural defects reduce emission intensity when they generate mid-gap states that provide nonradiative recombination pathways.²⁸ In a previous study of monolayer MoS₂, photoluminescence quenching (enhancement) near mirror (tilt) boundaries¹⁷ was attributed to increased (decreased) free carrier density near such boundaries, as would be produced by sulfur vacancies. If sulfur vacancies^{12,35} indeed cause quenching, one might expect to observe variations in photoluminescence intensity between samples of differing stoichiometry, and even within samples that are sulfur deficient. The group A, B, and C samples exhibit expected variations with decreasing sulfur stoichiometry. First, the samples have different morphologies that show the same trend with decreasing sulfur exposure as was previously reported by the Ajayan group.¹⁶ Additionally, group C samples show significant variations in PL intensity within individual

flakes, consistent with an increased sulfur vacancy concentration.

Structural defects and stoichiometry also have a strong influence on charge transport. Recent theoretical and experimental work has established that carrier mobilities and charge transport mechanisms in 2D MoS₂ depend strongly on carrier densities.^{5,36,38–40} Specifically, single-layer MoS₂ undergoes a metal to insulator transition as a function of carrier density. In the metallic state, the Fermi level is close to or above the mobility edge, while in the insulating state, the Fermi level is deep inside the band gap within a tail of localized states that gives rise to hopping transport.^{5,36,38} Indeed, capacitance–voltage and transport measurements by Zhu *et al.*²¹ on CVD MoS₂ devices with similar transfer characteristics to those described here identified the influence of localized (trap) states arising from structural defects. However, it has been established that S vacancies are sufficiently shallow to act as electron donors in MoS₂.^{41,42} For the particular distribution of defects present in these CVD grown films, it appears that the electron donation associated with sulfur vacancies makes a net positive contribution to the conductivity *via* both an increase in electron concentration and a related increase in field-effect mobility. We note that this counterintuitive result would not be expected for the introduction of sulfur vacancies in perfect materials with band transport.

Furthermore, the trends in mobility and carrier concentration cannot be readily explained in terms of variations in oxygen content. First, one would expect a decrease in conductivity upon formation or persistence of disordered insulating MoO₃ domains.⁴³ Second, replacement of residual oxygen atoms with sulfur atoms should actually increase the mobility, and replacement of residual oxygen atoms with vacancies could also improve the transconductance, from which the field-effect mobility is derived. Calculations of the scattering rates produced by substitutional oxygen and sulfur vacancies, as well as atomic level confirmation of the relative concentrations of each type of defect, would be useful in developing a more complete understanding of the factors that control mobility in CVD grown material.

We have shown here that the tuning of stoichiometry provides a useful degree of control over important device parameters, but it is important to consider what factors limit the performance of our materials in the context of recent work.^{17,18,21} Metal contacts do not have a dominant effect since field-effect mobilities extracted from 2-terminal and 4-terminal measurements of group A as well as group C devices are comparable. While the mobility of $\sim 20 \text{ cm}^2/(\text{V s})$ is the highest value reported for as-synthesized unencapsulated CVD monolayer MoS₂ crystals at room temperature, vacuum thermal annealing of CVD grown material has been shown to increase the field-effect

mobility up to $\sim 100 \text{ cm}^2/(\text{V s})$ at room temperature,²⁰ indicating room for further improvement. As noted above, capacitance–voltage and transport measurements by Zhu *et al.*²¹ on CVD MoS₂ devices with similar transfer characteristics to those described here identified the influence of localized (trap) states arising from structural defects. Trap states below the mobility edge reduce the transconductance even beyond the threshold voltage and likely lead to an underestimate of the free-carrier field-effect mobility of the present CVD MoS₂ transistors.

CONCLUSIONS

We summarize with three observations based on this work and the recent works discussed above. First,

stoichiometry variations contribute to unexpected variations in carrier mobilities. Second, since our stoichiometric (nonstoichiometric) flakes exhibit nominally better optical (electrical) properties, the optimal synthetic conditions cannot necessarily be deduced by electrical or optical measurements alone. Third, given the recent increases in mobility achieved by vacuum annealing,²⁰ a combined investigation of CVD growth conditions and post-growth annealing in vacuum and other environments is needed to assist in the identification of native defects and work toward their minimization in MoS₂ and other TMDCs. Atomically resolved studies involving annular dark field (ADF) STEM or scanning tunneling microscopy (STM) may prove useful in this regard.

METHODS

CVD Synthesis of Monolayer MoS₂ Flakes. Si wafers with 300 nm of thermally grown SiO₂ were cleaned in an O₂ plasma and used as growth substrates. Alumina boats containing solid MoO₃ (99%, Sigma-Aldrich) and S (99.95%, Sigma-Aldrich) powders were used as Mo and S precursors by placing in a 25 mm quartz tube in temperature zones of 800 and 150 °C, respectively. Growths were carried out at 150 Torr with He as the carrier gas (20 sccm). During the temperature ramp, the sulfur source (initially 3.85 in. away from the end of the tube) was loaded stepwise to 4.55, 4.95, and 5.25 in. away from the tube end when the temperature of the MoO₃ source reached 650, 725, and 800 °C, respectively. The growth was carried out for 10 min prior to cooling under a He flow.

X-ray Photoelectron Spectroscopy. XPS was conducted with a Thermo Scientific ESCA Lab 250Xi XPS with a monochromatic K α Al X-ray line. The probe size was $\sim 400 \mu\text{m}$ in diameter, nominally elliptical in cross section. A charge neutralization flood gun (Ar $^+$ ions) was used to compensate for local electrostatic fields on the MoS₂/SiO₂/Si samples. All elements within surveys were fitted with Shirley backgrounds. Core level spectra were charge corrected against fitted adventitious carbon at 284.8 eV. Subpeaks were fit using modified Shirley backgrounds and floating Gaussian–Lorentzian (GL) mixing. All subpeaks shared the same amount of GL character, but that amount was kept as a fitting parameter. Subpeaks were fit such that their full-width at half-maximum (fwhm) values were less than 3 eV. Core level spectra were collected at a pass energy of 100 eV and a dwell time of 100 ms.

Device Fabrication and Measurement. Field-effect transistors were fabricated on thermal oxide Si substrates (300 nm SiO₂) using standard e-beam lithography and lift-off processes. Metal contacts (2 nm Ti/70 nm Au) were thermally evaporated. After lift-off, devices were cleaned in *N*-methyl-2-pyrrolidone and deionized water to remove processing residues, which was observed to decreased hysteresis in MoS₂ transistors. All measurements were conducted in vacuum (pressure $< 2 \times 10^{-5}$ Torr) in a LakeShore CRX 4K probe station using Keithley source-meters and homemade LabVIEW programs. Four-terminal measurements were conducted by passing 10 nA current between electrode "1" and "4" in Figure 4a using Keithley 6430 source-meter and employing a remote preamplifier. Four-probe measurements of the devices in the subthreshold regime (Figure 4d) were not possible due to limits of input impedance of the instrument. Conductance versus gate voltage measurements of 4-terminal devices in the linear regime ($V > V_{th}$) were used to calculate the field-effect mobility.

Conflict of Interest: The authors declare no competing financial interest.

Acknowledgment. This work was supported by the Materials Research Science and Engineering Center (MRSEC) of

Northwestern University (National Science Foundation Grant DMR-1121262), NSF PREM Grant DMR-0934218, the Office of Naval Research (Grant N00014-14-1-0669), the Keck Foundation, and the Center for Hierarchical Materials Design (U.S. Department of Commerce, NIST 70NANB14H012). The microscopy work was supported by grants from the National Center for Research Resources (5 G12RR013646-12) and the National Institute on Minority Health and Health Disparities (G12MD007591) from the National Institutes of Health.

Supporting Information Available: AFM phase images of grain boundaries in MoS₂; effects of current annealing on MoS₂ devices; summarized electrical properties of MoS₂ devices. This material is available free of charge via the Internet at <http://pubs.acs.org>.

REFERENCES AND NOTES

- Sze, S. M.; Ng, K. K. *Physics of Semiconductor Devices*, 3rd ed.; Wiley: Hoboken, NJ, 2007.
- Jariwala, D.; Sangwan, V. K.; Lauhon, L. J.; Marks, T. J.; Hersam, M. C. Carbon Nanomaterials for Electronics, Optoelectronics, Photovoltaics, and Sensing. *Chem. Soc. Rev.* **2013**, *42*, 2824–2860.
- Jariwala, D.; Sangwan, V. K.; Lauhon, L. J.; Marks, T. J.; Hersam, M. C. Emerging Device Applications for Semiconducting Two-Dimensional Transition Metal Dichalcogenides. *ACS Nano* **2014**, *8*, 1102–1120.
- Radisavljevic, B.; Radenovic, A.; Brivio, J.; Giacometti, V.; Kis, A. Single-Layer MoS₂ Transistors. *Nat. Nanotechnol.* **2011**, *6*, 147–150.
- Jariwala, D.; Sangwan, V. K.; Late, D. J.; Johns, J. E.; Dravid, V. P.; Marks, T. J.; Lauhon, L. J.; Hersam, M. C. Band-like Transport in High Mobility Unencapsulated Single-Layer MoS₂ Transistors. *Appl. Phys. Lett.* **2013**, *102*, 173107.
- Late, D. J.; Huang, Y.-K.; Liu, B.; Acharya, J.; Shirodkar, S. N.; Luo, J.; Yan, A.; Charles, D.; Waghmare, U. V.; Dravid, V. P.; et al. Sensing Behavior of Atomically Thin-Layered MoS₂ Transistors. *ACS Nano* **2013**, *7*, 4879–4891.
- Perkins, F. K.; Friedman, A. L.; Cobas, E.; Campbell, P. M.; Jernigan, G. G.; Jonker, B. T. Chemical Vapor Sensing with Monolayer MoS₂. *Nano Lett.* **2013**, *13*, 668–673.
- Sangwan, V. K.; Arnold, H. N.; Jariwala, D.; Marks, T. J.; Lauhon, L. J.; Hersam, M. C. Low-Frequency Electronic Noise in Single-Layer MoS₂ Transistors. *Nano Lett.* **2013**, *13*, 4351–4355.
- Park, J. B.; France, C. B.; Parkinson, B. A. Scanning Tunneling Microscopy Investigation of Nanostructures Produced by Ar $^+$ and He $^+$ Bombardment of MoS₂ Surfaces. *J. Vac. Sci. Technol., B* **2005**, *23*, 1532–1542.
- Sengoku, N.; Ogawa, K. Investigations of Electronic Structures of Defects Introduced by Ar Ion Bombardments on

- MoS_2 by Scanning Tunneling Microscopy. *Jpn. J. Appl. Phys.* **1995**, *34*, 3363–3367.
11. Mann, J.; Ma, Q.; Odenthal, P. M.; Isarraraz, M.; Le, D.; Preciado, E.; Barroso, D.; Yamaguchi, K.; von Son Palacio, G.; Nguyen, A.; et al. 2-Dimensional Transition Metal Dichalcogenides with Tunable Direct Band Gaps: $\text{MoS}_{2(1-x)}\text{Se}_{2x}$ Monolayers. *Adv. Mater.* **2014**, *26*, 1399–1404.
 12. Ma, Q.; Isarraraz, M.; Wang, C. S.; Preciado, E.; Klee, V.; Bobek, S.; Yamaguchi, K.; Li, E.; Odenthal, P. M.; Nguyen, A.; et al. Post-Growth Tuning of the Bandgap of Single-Layer Molybdenum Disulfide Films by Sulfur/Selenium Exchange. *ACS Nano* **2014**, *8*, 4672–4677.
 13. Feng, Q.; Zhu, Y.; Hong, J.; Zhang, M.; Duan, W.; Mao, N.; Wu, J.; Xu, H.; Dong, F.; Lin, F.; et al. Growth of Large-Area 2d $\text{MoS}_{2(1-x)}\text{Se}_{2x}$ Semiconductor Alloys. *Adv. Mater.* **2014**, *26*, 2648–2653.
 14. Liu, K.-K.; Zhang, W.; Lee, Y.-H.; Lin, Y.-C.; Chang, M.-T.; Su, C.-Y.; Chang, C.-S.; Li, H.; Shi, Y.; Zhang, H.; et al. Growth of Large-Area and Highly Crystalline MoS_2 Thin Layers on Insulating Substrates. *Nano Lett.* **2012**, *12*, 1538–1544.
 15. Wu, S.; Huang, C.; Aivazian, G.; Ross, J. S.; Cobden, D. H.; Xu, X. Vapor–Solid Growth of High Optical Quality MoS_2 Monolayers with Near-Unity Valley Polarization. *ACS Nano* **2013**, *7*, 2768–2772.
 16. Najmaei, S.; Liu, Z.; Zhou, W.; Zou, X.; Shi, G.; Lei, S.; Yakobson, B. I.; Idrobo, J.-C.; Ajayan, P. M.; Lou, J. Vapour Phase Growth and Grain Boundary Structure of Molybdenum Disulphide Atomic Layers. *Nat. Mater.* **2013**, *12*, 754–759.
 17. van der Zande, A. M.; Huang, P. Y.; Chenet, D. A.; Berkelsbach, T. C.; You, Y.; Lee, G.-H.; Heinz, T. F.; Reichman, D. R.; Muller, D. A.; Hone, J. C. Grains and Grain Boundaries in Highly Crystalline Monolayer Molybdenum Disulphide. *Nat. Mater.* **2013**, *12*, 554–561.
 18. Lee, Y.-H.; Zhang, X.-Q.; Zhang, W.; Chang, M.-T.; Lin, C.-T.; Chang, K.-D.; Yu, Y.-C.; Wang, J. T.-W.; Chang, C.-S.; Li, L.-J.; et al. Synthesis of Large-Area MoS_2 Atomic Layers with Chemical Vapor Deposition. *Adv. Mater.* **2012**, *24*, 2320–2325.
 19. Kaasbjerg, K.; Thygesen, K. S.; Jacobsen, K. W. Phonon-Limited Mobility in *n*-Type Single-Layer MoS_2 from First Principles. *Phys. Rev. B* **2012**, *85*, 115317.
 20. Schmidt, H.; Wang, S.; Chu, L.; Toh, M.; Kumar, R.; Zhao, W.; Castro Neto, A. H.; Martin, J.; Adam, S.; Özyilmaz, B.; et al. Transport Properties of Monolayer MoS_2 Grown by Chemical Vapor Deposition. *Nano Lett.* **2014**, *14*, 1909–1913.
 21. Zhu, W.; Low, T.; Lee, Y.-H.; Wang, H.; Farmer, D. B.; Kong, J.; Xia, F.; Avouris, P. Electronic Transport and Device Prospects of Monolayer Molybdenum Disulphide Grown by Chemical Vapour Deposition. *Nat. Commun.* **2014**, *5*, 3087.
 22. Wu, J.; Schmidt, H.; Amara, K. K.; Xu, X.; Eda, G.; Özyilmaz, B. Large Thermoelectricity via Variable Range Hopping in Chemical Vapor Deposition Grown Single-Layer MoS_2 . *Nano Lett.* **2014**, *14*, 2730–2734.
 23. Wang, Q. H.; Kalantar-Zadeh, K.; Kis, A.; Coleman, J. N.; Strano, M. S. Electronics and Optoelectronics of Two-Dimensional Transition Metal Dichalcogenides. *Nat. Nanotechnol.* **2012**, *7*, 699–712.
 24. Splendiani, A.; Sun, L.; Zhang, Y.; Li, T.; Kim, J.; Chim, C.-Y.; Galli, G.; Wang, F. Emerging Photoluminescence in Monolayer MoS_2 . *Nano Lett.* **2010**, *10*, 1271–1275.
 25. Castellanos-Gomez, A.; Agrait, N.; Rubio-Bollinger, G. Optical Identification of Atomically Thin Dichalcogenide Crystals. *Appl. Phys. Lett.* **2010**, *96*, 213116.
 26. Brivio, J.; Alexander, D. T. L.; Kis, A. Ripples and Layers in Ultrathin MoS_2 Membranes. *Nano Lett.* **2011**, *11*, 5148–5153.
 27. Mak, K. F.; Lee, C.; Hone, J.; Shan, J.; Heinz, T. F. Atomically Thin MoS_2 : A New Direct-Gap Semiconductor. *Phys. Rev. Lett.* **2010**, *105*, 136805.
 28. Pankove, J. I. *Optical Processes in Semiconductors*; Courier Dover Publications: New York, 2012.
 29. Perera, M. M.; Lin, M.-W.; Chuang, H.-J.; Chamlagain, B. P.; Wang, C.; Tan, X.; Cheng, M. M.-C.; Tománek, D.; Zhou, Z. Improved Carrier Mobility in Few-Layer MoS_2 Field-Effect Transistors with Ionic-Liquid Gating. *ACS Nano* **2013**, *7*, 4449–4458.
 30. Chakraborty, B.; Bera, A.; Muthu, D. V. S.; Bhowmick, S.; Waghray, U. V.; Sood, A. K. Symmetry-Dependent Phonon Renormalization in Monolayer MoS_2 Transistor. *Phys. Rev. B* **2012**, *85*, 161403.
 31. Jahan, F.; Smith, B. E. Investigation of Solar Selective and Microstructural Properties of Molybdenum Black Immersion Coatings on Cobalt Substrates. *J. Mater. Sci.* **1992**, *27*, 625–636.
 32. Stewart, T. B.; Fleischauer, P. D. Chemistry of Sputtered Molybdenum Disulfide Films. *Inorg. Chem.* **1982**, *21*, 2426–2431.
 33. Anwar, M.; Hogarth, C. A.; Bulpett, R. Effect of Substrate Temperature and Film Thickness on the Surface Structure of Some Thin Amorphous Films of MoO_3 Studied by X-Ray Photoelectron Spectroscopy (ESCA). *J. Mater. Sci.* **1989**, *24*, 3087–3090.
 34. Baker, M. A.; Gilmore, R.; Lenardi, C.; Gissler, W. XPS Investigation of Preferential Sputtering of S from MoS_2 and Determination of MoS_x Stoichiometry from Mo and S Peak Positions. *Appl. Surf. Sci.* **1999**, *150*, 255–262.
 35. Quan, M.; Patrick, M. O.; John, M.; Duy, L.; Chen, S. W.; Yeming, Z.; Tianyang, C.; Dezheng, S.; Koichi, Y.; Tai, T.; et al. Controlled Argon Beam-Induced Desulfurization of Monolayer Molybdenum Disulfide. *J. Phys.: Condens. Matter* **2013**, *25*, 252201.
 36. Baugher, B.; Churchill, H. O.; Yang, Y.; Jarillo-Herrero, P. Intrinsic Electronic Transport Properties of High Quality Monolayer and Bilayer MoS_2 . *Nano Lett.* **2013**, *13*, 4212–4216.
 37. Liu, H.; Neal, A. T.; Ye, P. D. Channel Length Scaling of MoS_2 MOSFETs. *ACS Nano* **2012**, *6*, 8563–8569.
 38. Radisavljevic, B.; Kis, A. Mobility Engineering and a Metal–Insulator Transition in Monolayer MoS_2 . *Nat. Mater.* **2013**, *12*, 815–820.
 39. Ma, N.; Jena, D. Charge Scattering and Mobility in Atomically Thin Semiconductors. *Phys. Rev. X* **2014**, *4*, 011043.
 40. Ghatak, S.; Pal, A. N.; Ghosh, A. Nature of Electronic States in Atomically Thin MoS_2 Field-Effect Transistors. *ACS Nano* **2011**, *5*, 7707–7712.
 41. Qiu, H.; Xu, T.; Wang, Z.; Ren, W.; Nan, H.; Ni, Z.; Chen, Q.; Yuan, S.; Miao, F.; Song, F.; et al. Hopping Transport through Defect-Induced Localized States in Molybdenum Disulphide. *Nat. Commun.* **2013**, *4*, 2642.
 42. Kim, B. H.; Park, M.; Lee, M.; Baek, S. J.; Jeong, H. Y.; Choi, M.; Chang, S. J.; Hong, W. G.; Kim, T. K.; Moon, H. R.; et al. Effect of Sulphur Vacancy on Geometric and Electronic Structure of MoS_2 Induced by Molecular Hydrogen Treatment at Room Temperature. *RSC Adv.* **2013**, *3*, 18424–18429.
 43. Islam, M. R.; Kang, N.; Bhanu, U.; Paudel, H.; Erementchouk, M.; Tetard, L.; Leuenberger, M.; Khondaker, S. I. Electrical Property Tuning via Defect Engineering of Single Layer MoS_2 by Oxygen Plasma. *Nanoscale* **2014**, *6*, 10033–10039.